China Ocean Eng., Vol. 27, No. 2, pp. 141 – 158

DOI 10.1007/s13344-013-0013-0, ISSN 0890-5487

Wave-Tide-Surge Coupled Simulation for Typhoon Maemi*

Byung Ho Choi[a, 1], Byung Il Min[a], Kyeong Ok Kim[b] and Jin Hee Yuk[c]

[a] *Department of Civil and Environmental Engineering*, *Sungkyunkwan University*, *Suwon*, *440-746*, *Korea*

[b] *Marine Environments & Conservation Research Division*, *Korea Institute of Ocean Science & Technology*, *Ansan 426-744*, *Korea*

[c] *Supercomputing Center*, *Korea Institute of Science and Technology Information*, *Daejeon 305-806*, *Korea*

(Received 21 September 2012; received revised form 4 October 2012; accepted 16 November 2012)

ABSTRACT

The main task of this study focuses on studying the effect of wave-current interaction on currents, storm surge and wind wave as well as effects of current induced wave refraction and current on waves by using numerical models which consider the bottom boundary layer and sea surface roughness parameter for shallow and smooth bed area around Korean Peninsula. The coupled system (unstructured-mesh SWAN wave and ADCIRC) run on the same unstructured mesh. This identical and homogeneous mesh allows the physics of wave-circulation interactions to be correctly resolved in both models. The unstructured mesh can be applied to a large domain allowing all energy from deep to shallow waters to be seamlessly followed. There is no nesting or overlapping of structured wave meshes, and no interpolation is required. In response to typhoon Maemi (2003), all model components were validated independently, and shown to provide a faithful representation of the system's response to this storm. The waves and storm surge were allowed to develop on the continental shelf and interact with the complex nearshore environment. The resulting modeling system can be used extensively for prediction of the typhoon surge. The result show that it is important to incorporate the wave-current interaction effect into coastal area in the wave-tide-surge coupled model. At the same time, it should consider effects of depth-induced wave breaking, wind field, currents and sea surface elevation in prediction of waves. Specially, we found that: (1) wave radiation stress enhanced the current and surge elevation otherwise wave enhanced nonlinear bottom boundary layer decreased that, (2) wind wave was significantly controlled by sea surface roughness thus we cautiously took the experimental expression. The resulting modeling system can be used for hindcasting (prediction) the wave-tide-surge coupled environments at complex coastline, shallow water and fine sediment area like areas around Korean Peninsula.

Key words: *typhoon Maemi*; *finite element model*; *tide-surge-wave coupling*

1. Introduction

Typhoon Maemi, named after the Korean word for cicada, and the 14th typhoon in 2003, was the most powerful typhoon to hit the Korean Peninsula in a century. One of the hardest hit cities was Busan, the nation's largest port, where twelve of its 52 container lifting cranes were knocked down. It is remembered as the most powerful typhoon in the nation's history in terms of wind speed and air pressure. It landed on the coast of South Kyongsang Province on Aug. 12, with a central atmospheric pressure reaching 950 hPa which is lower than the previous record of 952 hPa. The typhoon also created a new record in terms of wind speed, by sending winds of up to 60 m/s, or about 135 miles per

* This study was supported in part by Brain Korea 21 Program for Sungkyunkwan University and the project for the development of the marine environmental impact prediction system funded by KIOST (Grant Nos. PE98743 and PE98818).
1 Corresponding author. E-mail: bhchoi.skku@gmail.com

hour, while passed through Jeju Island on Aug. 12.

Typhoon Maemi has been studied by several groups, but some problems still remain. The first one was caused by the leaking of metrological data for about 12 hours when typhoon Maemi (2003) passed through Korea. However, hindcasting and reanalysis data with six hour intervals were insufficient to resolve the typhoon features. The second one was caused by the leaking of ocean observation data; especially, the ocean wave buoy was not working reliably. Choi *et al*. (2007) studied typhoon Maemi by using the coupled model, which included the bottom boundary layer of Grant and Madsen (1979), as well as the two way interaction between the tide-surge and wave. The results showed a slightly underestimated typhoon surge due to the insufficient meteorological data set. Kawai *et al*. (2004) used the one way coupling system, which first computed the wave fields for computing the surface momentum transport. Chun *et al*. (2009) used a three-dimensional ocean model, POM (Princeton Ocean Model) and spectral wave model, WAM (Wave Modeling) in their study, where the WAM modified especially the refraction term for shallow conditions. The developed model accepted the 3D radiation stress suggested by Xie *et al*. (2004), which was extended based on the 2D radiation stress proposed by Longuet-Higgins and Stewart (1964). Their results were slightly underestimated for the wave heights, but the tide-surge was in a good agreement with the observed data.

We study the effect of wave-current interaction on currents, storm surge and wind wave as well as effects of current induced wave refraction and current on waves by using numerical models to improve insufficiencies of their studies. The bottom boundary layer and sea surface roughness parameter for shallow and smooth bed area around Korean Peninsula are considered in our model.

2. Numerical Method

2.1 Wind Wave Model

SWAN (Simulating WAves Nearshore) predicts the evolution in geographical space and time of the wave action density spectrum, with the relative frequency (σ) and the wave direction (θ), as governed by the action balance equation (Booij *et al*., 1999):

$$\frac{\partial N}{\partial t}+\nabla_{\vec{x}}\left[\left(\vec{\boldsymbol{c}}_{\mathrm{g}}+\vec{\boldsymbol{U}}\right)N\right]+\frac{\partial c_{\theta}N}{\partial\theta}+\frac{\partial c_{\sigma}N}{\partial\sigma}=\frac{S_{\mathrm{tot}}}{\sigma}. \tag{1}$$

The terms on the left-hand side represent, respectively, the change of wave action in time, t, the propagation of wave action in space (with $\nabla_{\vec{x}}$, the gradient operator in geographic space, $\vec{\boldsymbol{c}}_{\mathrm{g}}$, wave group velocity and $\vec{\boldsymbol{U}}$, the ambient current vector), depth and current induced refraction and approximate diffraction (with propagation velocity or turning rate c_{θ}), and the shifting of wave action due to variations in mean current and depth (with propagation velocity or shifting rate c_{σ}). The source term, S_{tot}, represents wave growth by wind; action lost due to whitecapping, surf breaking and bottom friction; and action exchanged between spectral components in deep and shallow water due to nonlinear effects. The associated SWAN parameterizations are given by Booij *et al*. (1999), with all subsequent modifications as present in version 40.72, including the phase-decoupled refraction/diffraction (Holthuijsen *et al*., 2003), although diffraction is not enabled in the present

simulations. The unstructured-mesh version of SWAN implements an analog to the four-direction Gauss-Seidel iteration technique employed in the structured version, and it maintains SWAN's unconditional stability (Zijlema, 2010). SWAN computes the wave action density spectrum at the vertices of an unstructured triangular mesh, and it orders the mesh vertices so it can sweep through them and update the action density using information from neighboring vertices.

2.2 Tide-Surge Model

ADCIRC (the ADvanced CIRCulation model) is a continuous-Galerkin, finite-element, shallow-water model that solves for water levels and currents at a range of scales (Luettich and Westerink, 2004). The details of this solution have been published widely (http://www.nd.edu/~adcirc/manual.htm to see Users Manual and Theory Report) and will not be restated here.

2.3 Sharing Information

SWAN is driven by wind speeds, water levels and currents computed at the vertices by ADCIRC. Marine winds can be input to ADCIRC in a variety of formats, and these winds are adjusted directionally to account for surface roughness (Bunya *et al*., 2010). ADCIRC interpolates spatially and temporally to project these winds to the computational vertices, and then it passes them to SWAN. The water levels and ambient currents are computed in ADCIRC before being passed to SWAN, where they are used to recalculate the water depth and all related wave processes (wave propagation, depth-induced breaking, etc.). The ADCIRC model is driven partly by radiation stress gradients that are computed with information from SWAN. These gradients, τ_s, waves are computed by:

$$\tau_{sx,\,\mathrm{wave}} = -\frac{\partial S_{xx}}{\partial x} - \frac{\partial S_{xy}}{\partial y}; \tag{2}$$

$$\tau_{sy,\,\mathrm{wave}} = -\frac{\partial S_{xy}}{\partial x} - \frac{\partial S_{yy}}{\partial y}, \tag{3}$$

where S_{xx}, S_{xy} and S_{yy} are the wave radiation stresses (Longuet-Higgins and Stewart, 1964; Battjes, 1972).

ADCIRC and SWAN run in series on the same local mesh and core. The two models "leap frog" through time, each being forced with information from the other model. Because of the sweeping method used by SWAN to update the wave information at the computational vertices, it can take much larger time steps than ADCIRC, which is diffusion- and also Courant time step limited due to its semi-explicit formulation and its wetting and drying algorithm. For that reason, the coupling interval is taken to be the same as the SWAN's time step. On each coupling interval, ADCIRC is run first, because we assume that, in the nearshore and the coastal floodplain, wave properties are more dependent on circulation. At the beginning of a coupling interval, ADCIRC can access the radiation stress gradients computed by SWAN at times corresponding to the beginning and end of the previous interval. ADCIRC uses that information to extrapolate the gradients at all of its time steps in the current interval. These extrapolated gradients are used to force the ADCIRC solution as described previously. Once the ADCIRC stage is finished, SWAN is run for one time step, to bring it to the same moment in time as ADCIRC. SWAN can access the wind speeds, water levels and currents computed

at the mesh vertices by ADCIRC, at times corresponding to the beginning and end of the current interval. SWAN applies the mean of those values to force its solution on its time step. In this way, the radiation stress gradients used by ADCIRC are always extrapolated forward in time, while the wind speeds, water levels and currents used by SWAN are always averaged over each of its time steps. The basic structure of this coupling system (ADCIRC+SWAN) was developed by Dietrich *et al*. (2010). A schematic of the communication is shown in Fig. 1.

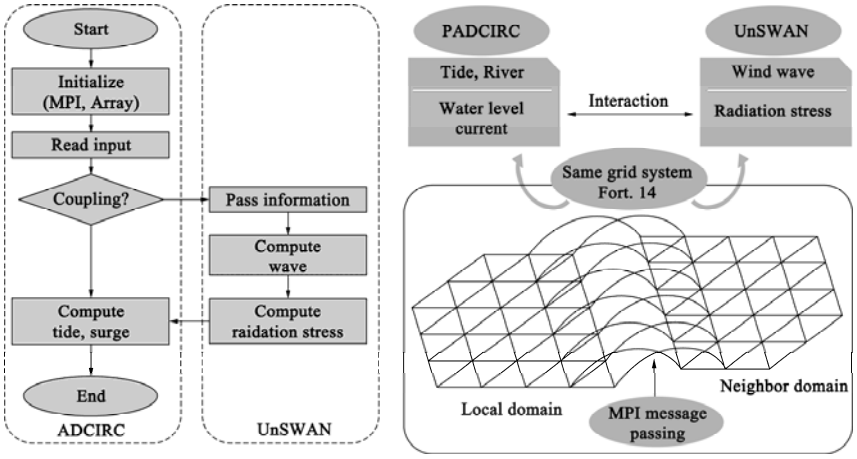

Fig. 1. Schematic of parallel communication between models and cores. Solid lines indicate communication for the edge-layer-based nodes between sub-meshes, and are intra-model and inter-core.

2.4 Bottom Boundary Layer

Before the 1980s, most scientists simply added the shear associated with waves and currents. However, Grant and Madsen (1979) formally extended the results because the non-linear interaction between the wave and current boundary layers caused the resultant bed shear-stresses to be greater than those that would result from a simple addition of the wave-alone and current-alone stresses. More than 20 theories and models have been proposed to describe bottom boundary layer. Soulsby (1997) performed a comparison of the eight bottom boundary layer models with 61 laboratory and 70 field values of the mean bed shear-stress during a wave cycle. It is revealed that no model performed better for all the criteria.

Model simulations were performed for two periods (5 and 10 s), 95 wave orbital velocities (0.05~1.00 m/s, 45 current velocities (0.05~0.50 m/s) and two wave-current angles (0º and 45º). The mean characteristics of the four wave-current bottom boundary layer models were evaluated by the mean bed stress as a non-dimensional bed, along with the Shield's parameter, given by

$$\theta_{\text{mean}} = \frac{\tau_{\text{mean}}}{(\rho_s - \rho) g d_{50}} . \tag{4}$$

The mean Shield's parameter, θ_{mean}, is calculated with the instantaneous bed stress over a wave period. Fig. 2 shows the predictions of the mean bed stress over a range of wave and mean current conditions. The mean Shields parameter is also predicted with wave bottom boundary layer models of Grant and Madsen (1979) (GM79 in Fig. 2), Styles and Glenn (2000) (SG00), Soulsby (1997) (S97)

and Soulsby and Clarke (2004) (SC04). All models showed an increase in the Shields parameter with increasing mean current velocity and wave orbital velocity. As the wave period was increased from 5 to 10 s, 30%~50% decreases were observed in the mean bed stress for relatively large mean current velocities.

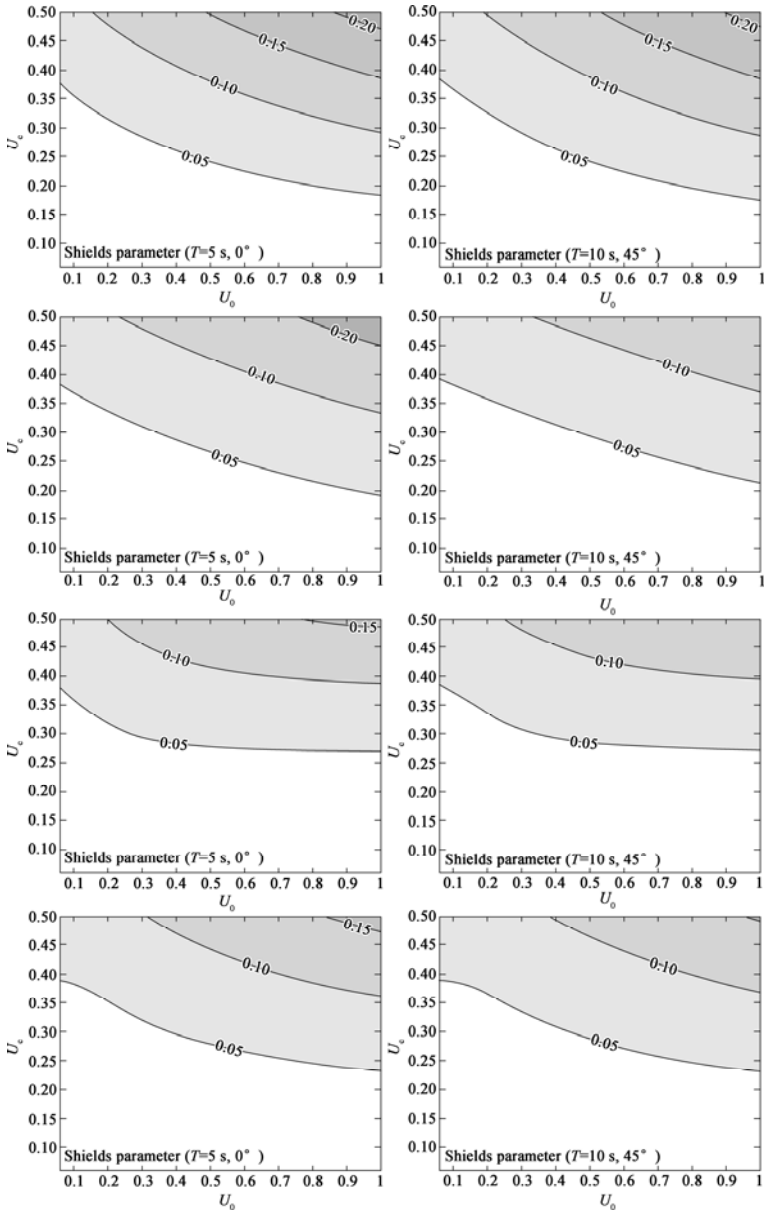

Fig. 2. Mean Shields parameter as a function of orbital wave velocity and mean current velocity for a wave period of 5 s (left panels) and 10 s (right panels). The figure shows the GM79 (Grant and Madsen, 1979), SG00 (Styles and Glenn, 2000), S97 (Soulsby, 1997) and SC04 (Soulsby and Clarke, 2004) from up to down.

Fig. 3 shows a further evaluation of the mean Shields parameter for the range of non-dimensional bed excursion defined by:

$$\frac{A}{k_n} = \frac{U_0 T}{2\pi k_0} . \tag{5}$$

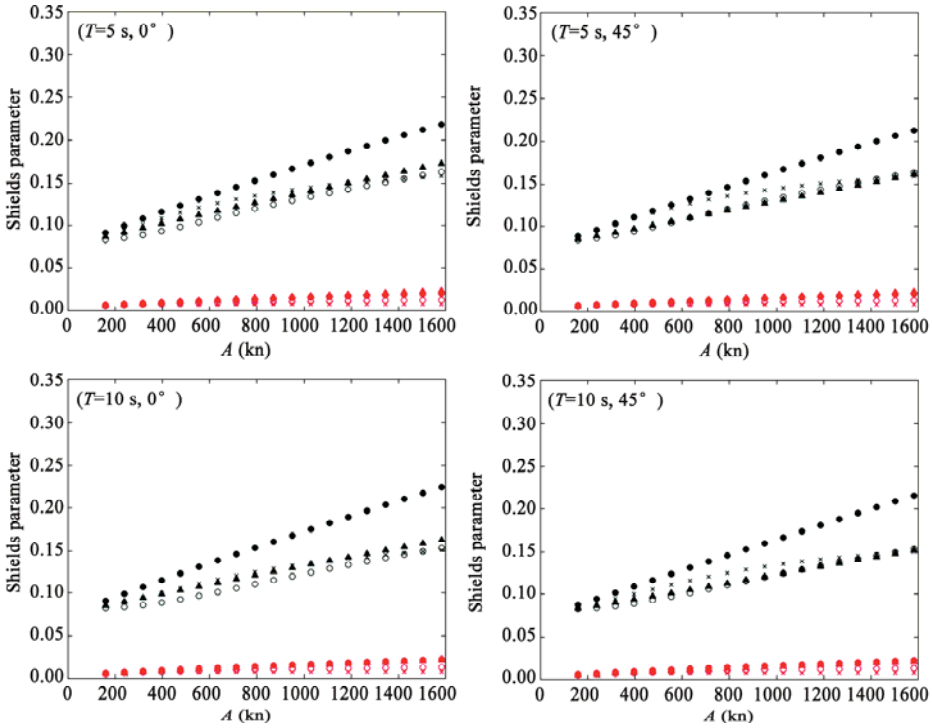

Fig. 3. Mean Shields parameter by GM79 (Grant and Madsen (1979); black circle), SG00 (Styles and Glenn (2000); triangle), S97 (Soulsby (1997); ×) and SC04 (Soulsby and Clarke (2004); white circle) for periods of 5 s (upper panels) and 10 s (lower panels), wave-current angles of 0º (left panels) and 45º (right panels), and mean currents 0.10 m/s (red) and 0.50 m/s (black).

For small wave periods and small mean currents all the models predicted low mean Shields parameter values, which were not sensitive to the wave bottom boundary layer. Grant and Madsen (1979) model predicted a larger wave period for non-dimensional bed orbital excursions. The predictions of Soulsby (1997), Soulsby and Clarke (2004) and Styles and Glenn (2000) asymptote at orbital excursion velocities greater than 1300. In other words, with a small Nikurades number, the three models showed similar values for the Shield's parameter. However, Grant and Madsen (1979) tended to overestimate the Shields parameter; whereas, the predictions continued to increase.

In this study, the Soulsby and Clarke (2004) model was adopted for the bed shear-stress under combined wave-current conditions. This model developed a simple analytical, non-iterative method for calculating the mean and maximum bed shear stress in combined wave and current flows. Most bottom boundary layer models have concentrated on the case of a rough turbulent flow, as would be found over a coarse sand or gravel bed, rather than the smooth turbulent flow commonly found over a mud bed, as found around the Korean Peninsula. Also, most theoretical predictors involve either an iterative solution or a full numerical model, which makes repeated calculation in the computational models of the hydrodynamics, sediment dynamics and the morpho-dynamics of estuaries and coastal areas excessively time-consuming. The bed stress should; therefore, preferably be predicted by using explicit

algebraic formulae.

The diameter of the surface sediment is an important component of bottom boundary layer models. However, information on the distribution of sediment is still very limited. In this study, data from previous works (Choi *et al*., 2005) were used.

2.5 Sea Surface Roughness

We have conducted eight sets of experiments with the coupled model. In the first experiment, this case is taken from an early version of the WAM Cycle 3 model (WAMDI group, 1988). It is suggested by Snyder *et al*. (1981), rescaled in terms of friction velocity u_* by Komen *et al*. (1984). The drag coefficient to relate u_* to the driving wind speed at 10 m elevation U_{10} is taken from Moon *et al*. (2007). In the second experiment, it is recommended by Janssen (1991) and it accounts explicitly for the interaction between the wind and the waves by considering atmospheric boundary layer effects and the roughness length of the sea surface. In other experiments, the original sea surface roughness parameterization has been replaced by the new parameterizations, where the sea surface roughness is calculated in spectral wave model. The new sea surface roughness parameterizations are as follows: Johnson *et al*. (1998) analyzed the mean dimensionless sea roughness from the field datasets from RASEX (Risø Air-Sea Experiment), and gave a trend of decreasing Charnock parameter with wave age. Smith *et al*. (1992) analyzed measurements of wind stress and waves collected during the HEXOS (Humidity Exchange over the Sea) experiment near a platform 9 km off the Dutch coast in a water depth of 18 m. They concluded from these measurements that the Charnock parameter decreases with increasing wave age. Oost *et al*. (2002) showed derivation of a connection between wave and the steepness of the waves thus, combination with the foregoing, between the Charnock parameter and the steepness. They used ASGAMAGE (Air Sea Gas, Marine Aerosol and Gas Exchange) data, like those from 1986 HEXMAX (the HEXOS Main Experiment) experiment. Extensive research at ECMWF (European Centre for Medium-Range Weather Forecasts) has shown that the sea-state dependent momentum transfer has resulted in improved forecast skill for both wind and waves. Table 1 shows the formulas of the sea surface roughness.

Table 1 Parameterizations of the sea surface roughness

Cases	Equations
Smith *et al*. (1992)	$z_0 = 0.48\left(c_p / u_*\right)^{-1}$
Johnson *et al*. (1998)	$z_0 = 1.89\left(c_p / u_*\right)^{-1.59}$
Oost *et al*. (2002)	$z_0 = 25 l_p / \pi\left(c_p / u_*\right)^{-4.5}$
ECMWF	$z_0 = 0.018\left(u_*^2 / g\right) + k \times 1.5 \times 10^{-5}$

3. Model Setup for Simulation of Typhoon Maemi (2003)

The complex mesh resolutions are shown in Fig. 4. This mesh incorporated local resolution down to 50 m, but also extended to the Yellow, East Seas and the western Pacific Ocean, including hundreds of islands, with the sufficient resolution of the wave-transformation zones near the coasts and intricate representation of various natural and man-made geographic features that collect and focus the storm surge in this region, and contained 260963 vertices and 472149 triangular elements.

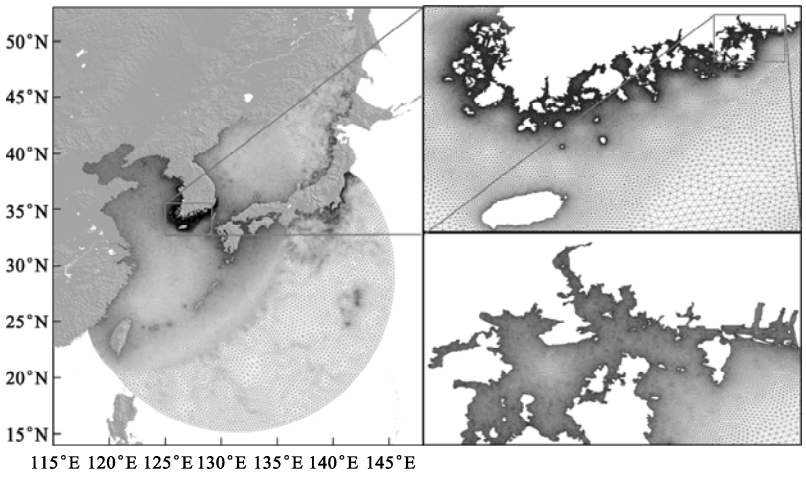

Fig. 4. Model domain with FEM mesh for the simulation of typhoon Maemi (2003).

Open boundary forcing was applied in the form of specifications based on NAO's (National Astronomical Observatory) tidal predictions (Matsumoto *et al*., 2000) along the model's open water boundary. The sea level pressures and wind field, which were predicted by RDAPS (Regional Data Assimilation and Prediction System)/KMA (Korea Meteorological Administration), seemed to be unsuitable for storm surge simulations. Meteorological data sets collected through using RDAPS/KMA at three hour intervals were insufficient because the path of typhoon Maemi to the southern part of Korea just took six hours (Fig. 5). Therefore, the RDPAS/KMA data set and Holland Parameter model were coupled to improve the typhoon center pressure and maximum wind. The methods may be blended like utilizing a dynamical model solution as a background into which observations or inner-core kinematically analyzed winds may be assimilated. In this study, we choose the RDAPS/KMA data set for background and Holland Parameter model (Eqs. (6) and (7)) for inner-core. Through a comparison of the observation, we choose the Holland 'B' parameter as 0.786 (Kang *et al*., 2002) and radius of inner core as two times of maximum storm radius.

$$P_r = P_0 + \Delta P \exp\left[-(R_{\max}/r)^B\right], \tag{6}$$

where, the Holland Parameter 'B' is an exponent factor that specifies the shape of the radial pressure profile, P_r is the surface pressure at a distance r from the typhoon center, P_0 is the central pressure, and ΔP is the difference between the peripheral pressures. The gradient balance velocity V_g for a stationary storm is thus

$$V_g = \left\{ \left(\frac{R_{\max}}{r}\right)^B \frac{B\Delta P \exp\left[-\left(\frac{R_{\max}}{r}\right)^B\right]}{\rho} + r^2 f^2 \right\}^{1/2} - \frac{fr}{2}, \tag{7}$$

where, ρ is the density of air and f is the Coriolis parameter.

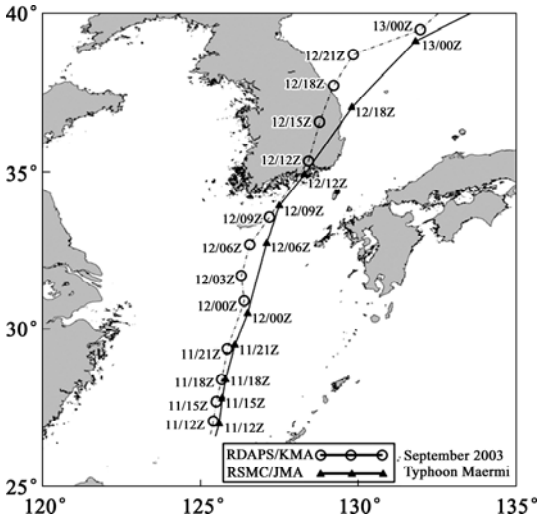

Fig. 5. Best tracks of typhoon Maemi (2003) by RDAPS/KMA and RSMC/JMA.

Fig. 6 shows the RDPAS/KMA and blended data sets in the left and right columns, respectively, and Fig. 7 shows the comparisons of the measured pressure and wind speed between the RDAPS/KMA and blended data sets. The blended data set was close to the measured data, but over-estimated in Seoquipo Station due to the geophysical effect from Hanra Mountain, Jeju.

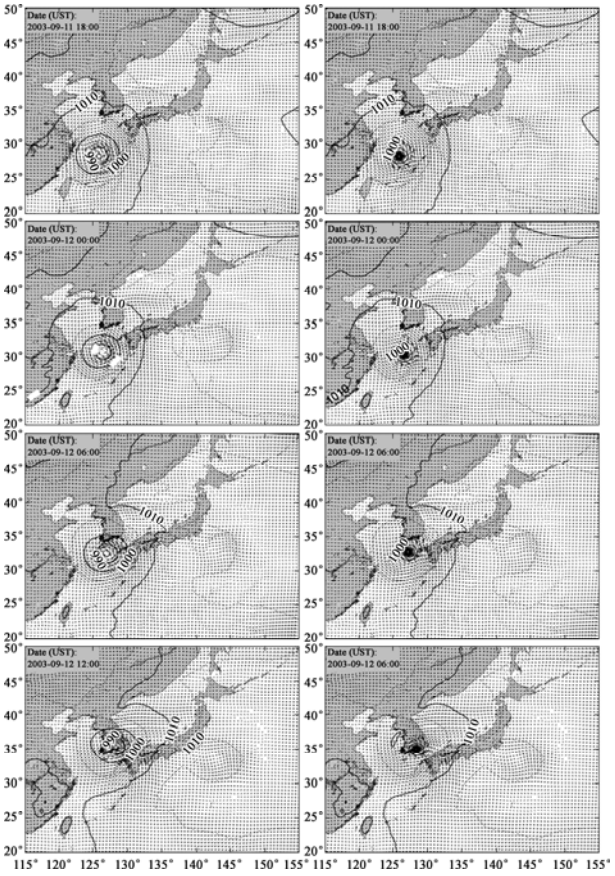

Fig. 6. Typhoon Maemi's wind speed vector (10 m wind; m/s) and pressure contour (mean sea level pressure; hPa) at six hour interval from 18:00 UTC Sep. 11, 2003 (from up to down). The left panels show the RDAPS/KMA ((1/12)º) and the right panels show the blended data with Holland Parameter model and RDAPS/KMA ((1/12)º).

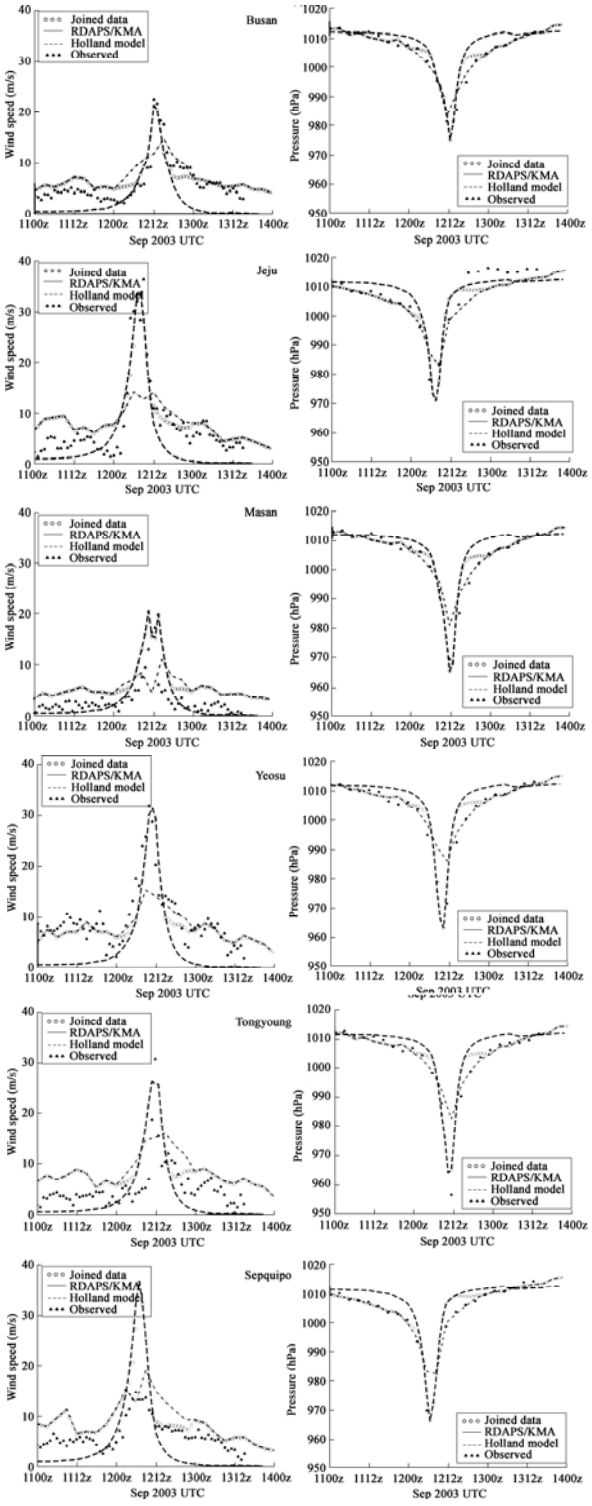

Fig. 7. Observed wind speed and pressure, RDAPS/KMA and blended data.

4. Simulation Results

4.1 Storm Surge

To validate the surge-tide-wind wave, we compared the model results with measurements carried out by KHOA (Korea Hydrographic and Oceanographic Administration). KHOA collected and analyzed water level measurements at eight stations, and Ieodo, Busan and Ulsan Ports with four pressure wave gauges, as shown in Fig. 8.

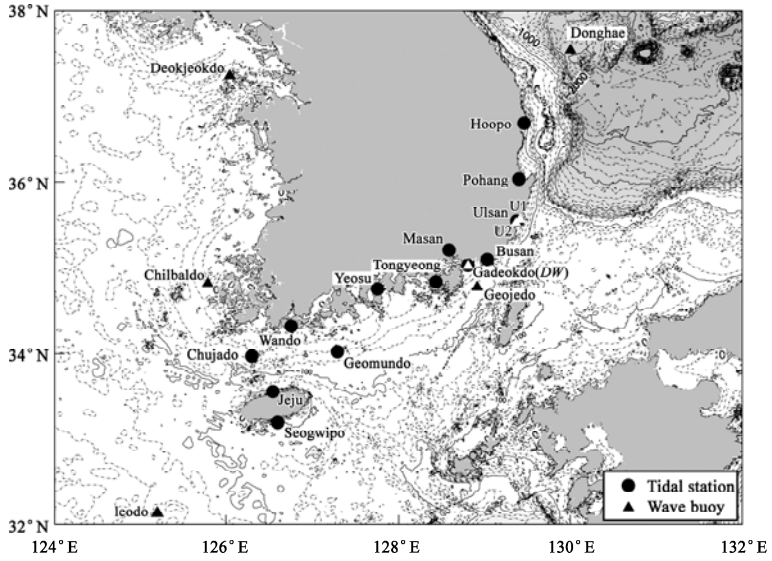

Fig. 8. Locations of the tidal stations used for the near shore tide-surge validation of ADCIRC and wave stations used for wave validation of SWAN during typhoon Maemi.

The Korean Peninsula is surrounded by the Yellow Sea to the West Sea, the South Sea, and the East Sea on the east. The Yellow Sea (shallow inland sea lying between northeastern China and the Korean Peninsula), the South Sea of Korea, and the East Sea show different characteristics in topographical aspects (Fig. 8). The Yellow Sea and the South Sea of Korea have shelf seas with maximum depths of less than 100 m, while the bottom conditions in the Yellow Sea are largely different from those in the South Sea of Korea (Choi *et al*., 2005). The very large amount of sediment input from the major rivers might be expected to deposit mud and fine grained sediments. The East Sea has a mean depth of over 1000 m.

Several numerical experiments with or without the effect of surge, tide, and wind were carried out in this study, and then compared with the above measurement dataset (Figs. 9~13). We calculated storm surge by the meteorological data without the influence of tide and wind wave (symbol 'S' in Figs. 9~13). Similarly, the symbol 'W' indicates the computed wind wave without the effect of tidal current and changes of water heights. The symbol 'TS' indicates the consideration of tide effect on the experiment 'S'. The symbol 'WTS' means the consideration of wind wave on the experiment 'TS' and the letters in the parentheses indicate the sea surface roughness applied in the experiment. All the experiments have been applied the bottom boundary layer model (Soulsby and Clarke, 2004). Additionally, we carried out the experiment by using the bottom boundary layer model proposed by

Soulsby and Clarke (2004) to evaluate the effect of radiation stress on the current ('WTSB' in Fig. 13). Note that 'WTS' indicates that the bottom friction is calculated by the drag law in Fig. 13.

The water levels at Busan Station on the east side of the typhoon track were within 0.1 m of the measured values, showing excellent agreements in terms of timing and hydrographic features (Fig. 9). In Tongyoung and Yeosu Stations on the west side of the typhoon track, the water level showed a good agreement in the timing of the peaks and rising and drainage rates. The values measured at Masan Station showed a largely negative surge about nine hours before the peak surge arrived, but the model results cannot capture this negative surge.

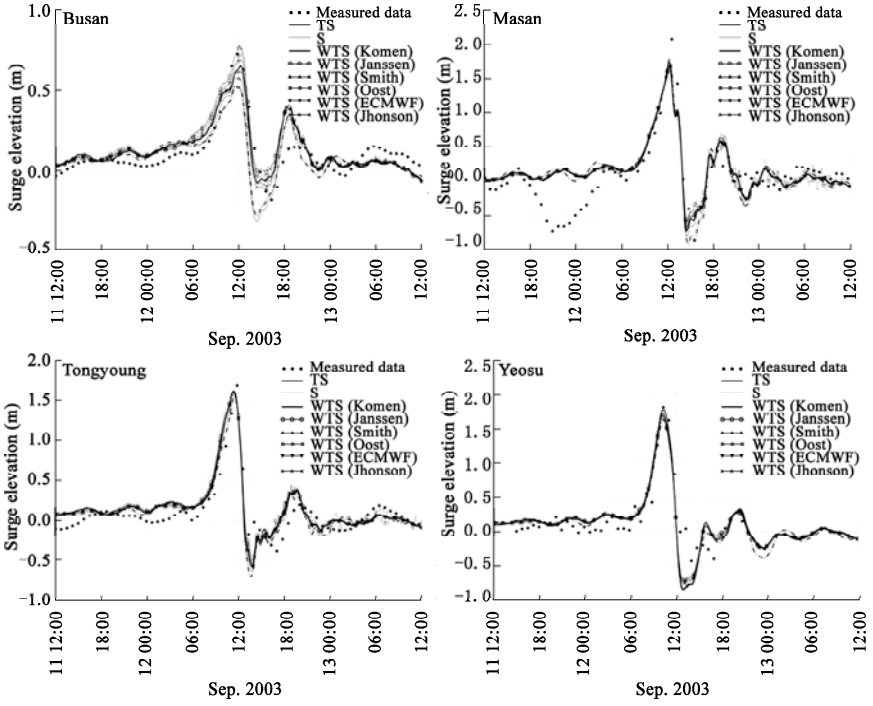

Fig. 9. Typhoon surge elevation during typhoon Maemi.

The surge values computed at Masan Station with the uncoupled system, and 'TS', showed more or less the same trends as those computed with the coupled system. However, the surge values computed with the uncoupled version tended to be about 5% smaller, as shown in the lower left panel of Fig. 9. The influence of using a coupled system was larger at Yeosu and Busan Stations. The differences of the surge elevations between the results from the coupled and uncoupled implementations ranged from 10 to 20 cm during storm events; about three times larger than the differences between the tide and tide-surge simulations. The best estimations of the surge elevation (about 0.17, 0.56 and 0.79 m, respectively) were larger than those computed at Busan, Yeosu and Tongyoung Stations; the values also tended to improve from the uncoupled to coupled system. At Masan Station, the effect of coupling on the surge elevation was similar to those observed at Busan, Yeosu and Tongyoung Stations. Also, there is an overestimation of the surge elevation due to the surface roughness (Janssen, 1991; Oost *et al*., 2002), but Oost *et al*. (2002) showed the best result in

the case of Busan Station.

4.2 Storm Wave

The simulated significant wave height, mean period and mean wave direction were compared with the observations and a good agreement was found between the observed and simulated data. Fig. 10 shows the observed significant wave height against those simulated from the six experiments. The effect of the sea surface roughness on the simulated wave fields in each experiment was evident compared with Komen *et al*. (1984), with the significant wave height simulated by each surface roughness being very close to the SWH (significant wave height) observed at Gaduck-Island (Gaduckdo), where the station was very shallow; thus, the wave height was controlled by the wave breaking. At both U1 and U2 Stations of Ulsan which were located on the right side of the typhoon track, the results of Oost *et al*. (2002) and Janssen (1991) overestimated, Smith *et al*. (1992) underestimated the wave heights, and Johnson *et al*. (1998) which is based on the theory of wave age showed a good agreement. Also, the result of 'ECMWF' showed a good agreement with observations. Ieodo Station was located to the left side of typhoon Maemi (2003) and at a depth of 50.0 m. Smith *et al*. (1992) and Johnson *et al*. (1998) showed a good agreement for the low wind situation before the typhoon passed the station on Sep. 11, 2003, but the experiments based on other theories (Charnock like, wave age and effect of swell) overestimated. However, the wave age theory underestimated the peak wave height under the strong wind condition; in contrast the other theories satisfactorily reproduced the peak wave height.

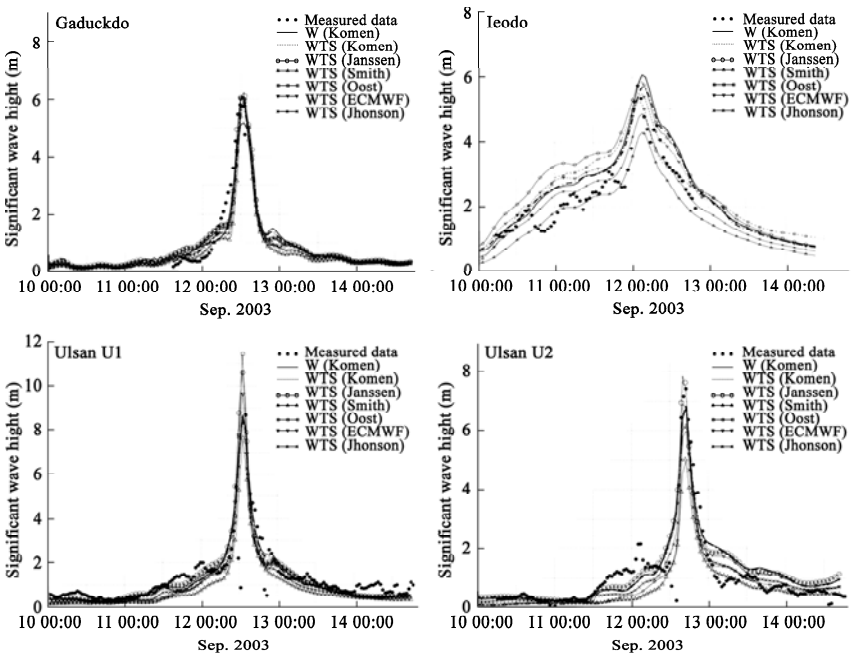

Fig. 10. Significant wave heights during typhoon Maemi at three pressure wave gauges (Gaduckdo, Ulsan and Ieodo). The measured data are shown with black dots, the numerical results are shown with solid lines, the wave growth term has been adopted by Komen *et al*. (1984), and other numerical results of expression about sea surface roughness are shown by several symbols.

Fig. 11 shows the simulated wave period (TM01) against the observed significant wave period. Komen *et al*. (1984) showed underestimations at all the observed stations. Also, the variation of the wave period was large via the other theory (quasi-linear theory) at the Gaduckdo Station. The quasi-linear theory overestimated the wave period at U1 and U2 Stations of Ulsan before the affect of the typhoon. However, the peak value was satisfactorily reproduced by the Oost *et al*. (2002) and Janssen (1991). All the theories underestimated the wave period after the typhoon had passed the station, which shows the importance of good background meteorological data.

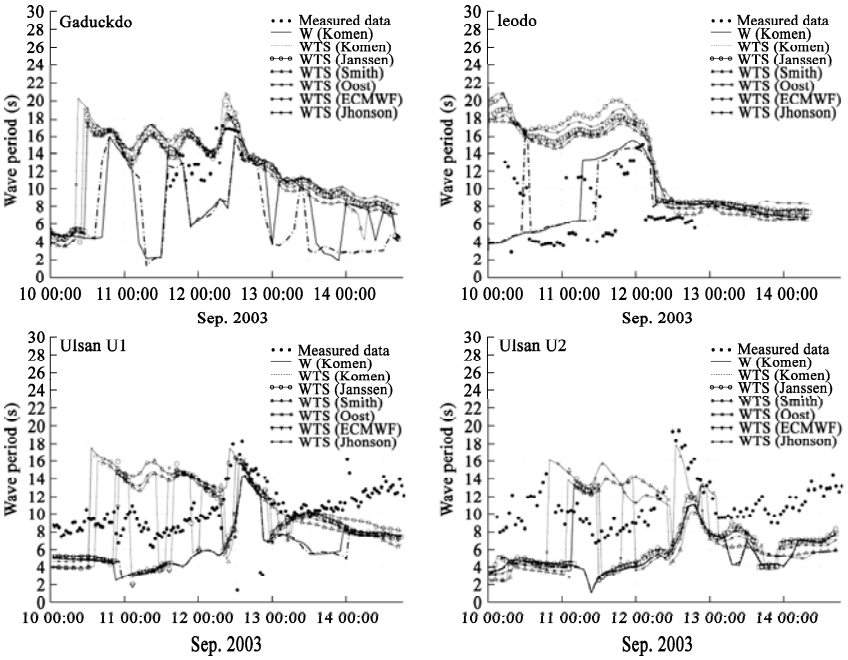

Fig. 11. Wave period during typhoon Maemi at three pressure wave gauges (Gaduckdo, Ulsan and Ieodo). The measured data are shown with black dots, the numerical results are shown with solid lines, the wave growth term has been adopted by Komen *et al*. (1984), and other numerical results of expression about sea surface roughness are shown in several symbols.

Fig. 12 shows the comparison of mean wave directions. The experiments based on all the theories show a good agreement except the wave age theory (Smith *et al*., 1992). The difference of about 90º was found during the developing stage.

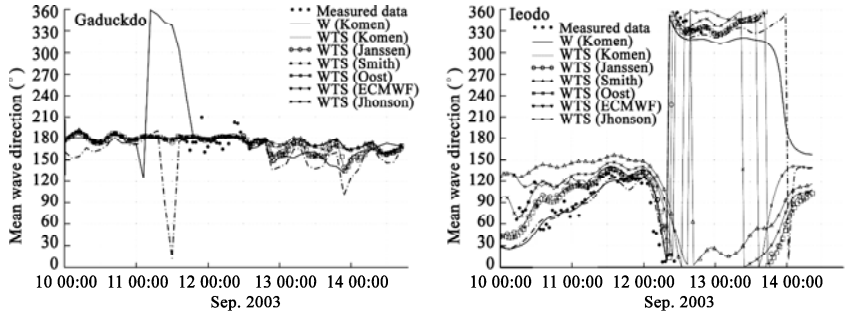

Fig. 12. Mean wave direction during typhoon Maemi at pressure wave gauges of Gaduckdo and Ieodo. The measured data are shown with black dots, the numerical results are shown with solid lines, the wave growth term has been adopted by Komen *et al*. (1984), and other numerical results of expression about sea surface roughness are shown by several symbols.

4.3 Effect on Current

The excessive momentum flux (or radiation stress) associated with the presence of waves on the hydrodynamics was also evaluated. The excessive current for the evaluation of the radiation stress effect was computed by subtracting the standard fully coupled implementation, i.e. two way interactions, from the fully coupled version that includes radiation stress terms. The inclusion of radiation stress in the momentum equation produces an excessive flow of the same order of magnitude as that produced when considering a radiation stress formulation (see Fig. 13). The current pattern was similar to that considering the effect of coupling.

The excessive currents related to the effect when a wave-dependent drag coefficient is considered in the computation of the surface stress are shown in Fig. 13. During the main events, the magnitude of this effect was observed to be in 10 ~ 40 cm/s (Yeosu and Busan Stations), representing about 40% of the typical current speed at the observation position. The generally modified current direction followed the direction of the radiation stress, with excessive currents flowing toward the northeast during the southwesterly wave conditions and toward the southwest during the northerly wave conditions. These patterns were disrupted during the strongest southwesterly surge event (between 06:00 and 12:00 September 12) at stations which are closer to the coast, especially Masan Station, where the current flows in the opposite direction to the general pattern; thus, the magnitude decreased. Current maxima were observed during this period, which were well correlated with the maxima of the surge differences at each station.

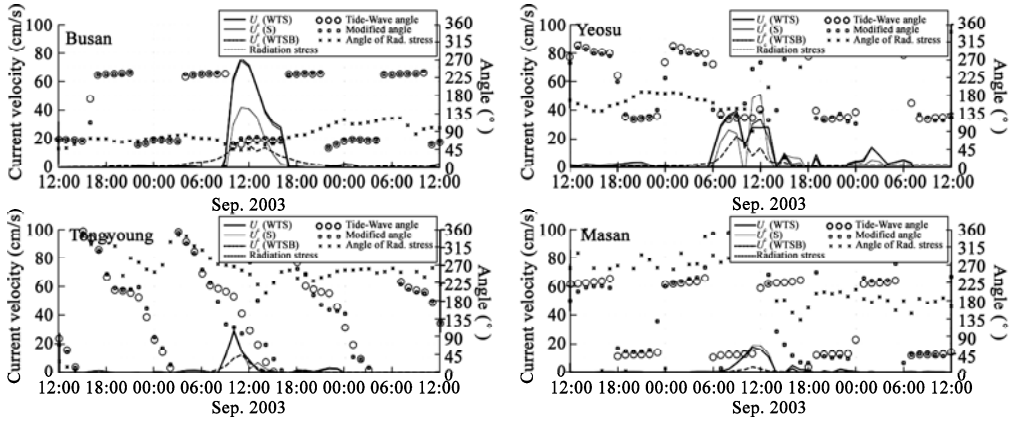

Fig. 13. Angle of tide and wave (○), modified angle of tide and wave due to interaction (□), angle of radiation stress (×), and magnitudes of current velocity (U_c) (wave-tide-surge ('WTS'), surge ('S'), wave-tide-surge-BBL ('WTSB')).

4.4 Effect of Topography

Fig. 14 shows the distribution indicating an increase rate of the sea elevation rise due to the gradient of radiation stress. The maximum surge elevation was increased by 5% to 12% due to the gradient of radiation stress at shallow water area near the coastline. The wave was not influenced by the bottom topography at the deep sea, and it did not change the energy gradient. But in the shallow sea where they were influenced by the bottom topography, the gradient of radiation stress began to change by a transition of the wave energy distribution due to dissipation and refraction. Fig. 15 shows the distribution of the significant wave height (gray dot line), direction of peak wave (gray vector),

water level (black line) and current velocity (black vector) of the typhoon landed in the land at the time of September 12, 2003. As shown in Fig. 15, most of the area from the direction of water waves and current are different from each other and each place of ocean wave and storm surge located at different area. The storm surge changes the total water level, if the total water level is shallower than still water level. The wind wave may be affected by the bottom and vice versa. Also, the transition of the wave energy distribution due to the change of total water depth is trigger to change the gradient of radiation stress. Therefore the change makes additional stress at the background ocean tide and surge, as a result the background current and water level being changed. In the actual phenomenon, background flow can make change of the wavelength and wave steepness of the surface wind waves. Amount of transferred energy from wind to ocean and surface wind wave is available to be changed, because the sea surface roughness generally described by the wave age, wave length and wave steepness given the phenomenon due to the impact on the amount of energy transferred from the wind can affect. The used mesh incorporated local resolution down to 50 m, and thus well represented various physical phenomena of wave-tide-surge at the wave-transformation zones near the coasts and complex coastal areas including hundreds of islands. In particular, the gradient of radiation stress is greatly influenced by the horizontal resolution; therefore, as mentioned above, the FEM system is well appropriate to study ocean systems around the Korea peninsula.

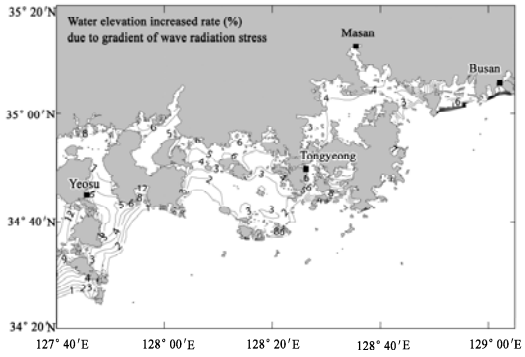

Fig. 14. Distribution of changed water level by radiation stress effect. The unit is ratio (%) of wave-tide-surge coupled simulation by tide-surge simulation.

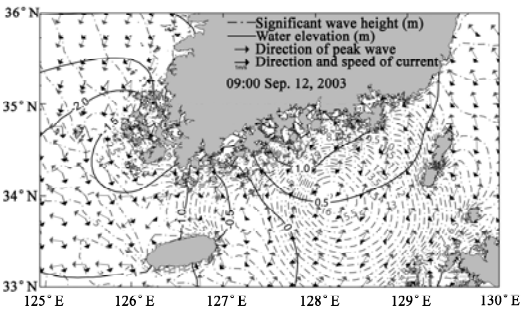

Fig. 15. Distribution of background water elevation and current by tide and surge (black line and arrow), the unit vector of direction of peak wave and significant wave height (gray).

5. Conclusions

In response to typhoon Maemi (2003), ADCIRC was coupled with SWAN spectral wave models. This coupling was beneficial; all model components were validated independently, and shown to provide a faithful representation of the system's response to these two storms. Waves and storm surges were allowed to develop on the continental shelf and interact with the complex nearshore environment. The resulting modeling system was used extensively for the prediction of the typhoon surge.

The surge elevation and current were significantly changed by the wave radiation stress in the shallow water area. Also, the fully coupled simulation reproducing the surge elevation well agreed with the observed data, but the uncoupled simulation tended to underestimate. In particular, at the Ieodo Station which was not affected by the land topography, the mean wave direction was opposite to

those of the coupled and uncoupled experiments. The mean wave direction in the coupled experiment showed a good agreement with the observed data.

In this research, the importance of the wind source term was reviewed, and the quasi-linear theory showed different wave fields following the sea surface roughness. Oost *et al*. (2002) introduced the wave length (the importance of swell in estimating the surface roughness) and wave age as components of the sea surface roughness and our result also showed a good agreement in the case of typhoon Maemi hindcasting.

The importance of the bottom boundary layer has been discussed, but it is not easy to prove the accuracy of these physical features; however, when the combined nonlinear effect of bottom stress under wave-current conditions is not involved the results then over-estimated the surge elevation; especially, the quasi-linear theory is adopted for the experiments. We should be careful to consider the bottom boundary layer in the wave-tide-surge coupled system. If this term is not considered, overestimations of the surge elevation and current velocity can occur. The radiation stress, wind energy transport and bottom boundary layer effects must also be taken into account for experiments related to the wind wave and storm surge.

Although the above terms are involved in a numerical system so the consumption of computational resources always increases, the future works must aim at creating the forecasting system based on the wave-tide-surge coupled model in this study.

References

Battjes, J. A., 1972. Radiation stresses in short-crested waves, *Journal of Marine Research*, **30**(1): 56~64.

Booij, N., Ris, R. C. and Holthuijsen, L. H., 1999. A third-generation wave model for coastal regions, Part I, Model description and validation, *J. Geophys. Res*., **104**(C4): 7649~7666.

Bunya, S., Dietrich, J. C., Westerink, J. J., Ebersole, B. A., Smith, J. M., Atkinson, J. H., Jensen, R., Resio, D. T., Luettich, R. A., Dawson, C., Cardone, V. J., Cox, A. T., Powell, M. D., Westerink, H. J. and Roberts, H. J., 2010. A high resolution-coupled riverine flow, tide, wind, wind wave, and storm surge model for southern Louisiana and Mississippi, Part I: Model development and validation, *Monthly Weather Review*, **138**(2): 345~377.

Choi, B. H., Mun, J. Y. and Ko, J. S., 2005. Wintertime suspended sediment simulation in the Huanghai and East China Seas, *Acta Oceanologica Sinica*, **24**(1): 46~59.

Choi, B. H., Kim, D. C., Kim, H. S. and Kim, Y. B., 2007. Wave-tide-surge coupled model simulation for typhoon Maemi, *Acta Oceanologica Sinica*, **26**(1): 35~47.

Chun, J., Ahn, K. and Yoon, J.-T., 2009. Development of the combined typhoon surge-tide-wave numerical model application to shallow water: 2. Verification of the combined model for the case of Typhoon Maemi, *Journal of Korean Society of Coastal and Ocean Engineers*, **21**(1): 79~90. (in Korean)

Dietrich, J. C., Bunya, S., Westerink, J. J., Ebersole, B. A., Smith, J. M., Atkinson, J. H., Jensen, R., Resio, D. T., Luettich, R. A., Dawson, C., Cardone, V. J., Cox, A. T., Powell, M. D., Westerink, H. J. and Roberts, H. J., 2010. A high-resolution coupled riverine flow, tide, wind, wind wave and storm surge model for southern Louisiana and Mississippi, Part II: Synoptic description and analyses of Hurricanes Katrina and Rita, *Monthly Weather Review*, **138**, 378~404.

Grant, W. D. and Madsen, O. S., 1979. Combined wave and current interaction with a rough bottom, *J. Geophys. Res*., **84**(C4): 1797~1808.

Holthuijsen, L. H., Herman, A. and Booij, N., 2003. Phase-decoupled refraction−diffraction for spectral wave models, *Coast*. *Eng*., **49**(4): 291~305.

Janssen, P. A. E. M., 1991. Quasi-linear theory of wind-wave generation applied to wave forecasting, *Journal of Physical Oceanography*, **21**(11): 1631~1642.

Johnson, H. K., Højstrup, J., Vested, H. J. and Larsen, S. E., 1998. On the dependence of sea surface roughness on wind waves, *Journal of Physical Oceanography*, **28**, 1702~1716.

Kang, S. W., Jun, K. C., Bang, G. H. and Park, K. S., 2002. Empirical relationship between central pressure and maximum sustained wind for tropical cyclones in northeast Asian Sea, *Korean Journal of the Atmospheric Sciences*, **38**(5): 523~530.

Kawai, H., Tomita, T., Hiraishi, T., Kim, D.-S. and Kang, Y. K., 2004. Hindcasting of storm surge by Typhoon 0314 (Maemi), In: Choi, B. H. (ed.), *Workshop Proceedings on Waves and Storm Surges around Korean Peninsula*, Hamrimwon Publishing Co., South Korea, 67~73.

Komen, G. J., Hasselmann, S. and Hasselmann, K., 1984. On the existence of a fully developed wind-sea spectrum, *Journal of Physical Oceanography*, **14**(8): 1271~1285.

Longuet-Higgins, M. S. and Stewart, R. W., 1964. Radiation stresses in water waves; physical discussions, with applications, *Deep Sea Research and Oceanographic Abstracts*, **11**(4): 529~562.

Luettich, R. A. and Westerink, J. J., 2004. *Formulation and Numerical Implementation of the 2D/3D ADCIRC Finite Element Model*, Version 44.XX, http://adcirc.org/adcirc_theory_2004_12_08.pdf.

Matsumoto, K., Takanezawa, T. and Ooe, M., 2000. Ocean tide models developed by assimilating TOPEX/POSEIDON altimeter data into hydrodynamical model: A global model and a regional model around Japan, *Journal of Oceanography*, **56**(5): 567~581.

Moon, I. J., Ginis, I., Hara, T. and Thomas, B., 2007. A physics-based parameterization of air-sea momentum flux at high wind speeds and its impact on hurricane intensity predictions, *Monthly Weather Review*, **135**, 2869~2878.

Oost, W. A., Komen, G. J., Jacobs, C. M. J. and Vanoort, C., 2002. New evidence for a relation between wind stress and wave age from measurements during ASGAMAGE, *Boundary-Layer Meteorology*, **103**(3): 409~438.

Smith, S. D., Anderson, R. J. Oost, W. A., Kraan, C., Maat, N., de Cosmo, J., Katsaros, K. B., Davidson, K. L., Bumke, K., Hasse, L. and Chadwick, H. M., 1992. Sea surface wind stress and drag coefficients: the HEXOS results, *Boundary-Layer Meteorology*, **60**(1-2): 109~142.

Snyder, R. L., Dobson, F. W., Elliott, J. A. and Long, R. B., 1981. Array measurement of atmospheric pressure fluctuations above surface gravity waves, *Journal of Fluid Mechanics*, **102**(1): 1~59.

Soulsby, R. L., 1997. *Dynamics of Marine Sands*: *A Manual for Practical Applications*, Thomas Telford, London, UK.

Soulsby, R. L. and Clarke, S., 2004. *Bed Shear-Stresses Under Combined Waves and Currents on Smooth and Rough Beds*, Report TR 137, HR Wallingford Ltd., Wallingford, UK.

Styles, R. and Glenn, S. M., 2000. Modeling stratified wave and current bottom boundary layers on the continental shelf, *J*. *Geophys*. *Res*., **105**(C10): 24119~24139.

WAMDI group, 1988. The WAM model−A third generation ocean wave prediction model, *Journal of Physical Oceanography*, **18**(12): 1775~1810.

Xie, L., Pietrafesa, L. and Peng, M. C., 2004. Incorporation of a mass-conserving inundation scheme into a three dimensional storm surge model, *Journal of Coastal Research*, **20**, 1209~1223.

Zijlema, M., 2010. Computation of wind-wave spectra in coastal waters with SWAN on unstructured grids, *Coast*. *Eng*., **57**(3): 267~277.